EUROPEAN ORGANIZATION FOR NUCLEAR RESEARCH
CERN — A&B DIVISION

AB-Note-2007-034 BI

CERN-NUFACT-Note-153

Compressor Lattice Design for SPL Beam

M. Aiba

Abstract

A compressor ring providing very short proton bunches of a few ns has been designed as a component of a proton driver in the neutrino factory. Proton beams accelerated with the SPL (Superconducting Proton Linac) are stored in an accumulator ring before being transported to a compressor ring. The bunch compression is then performed with longitudinal phase rotation. For the neutrino factory, a special pulse structure of the primary proton beam is required. In the SPL based proton driver, the specification imposes that six (or five) bunches of a few ns length and about 12μs bunch spacing are formed in one cycle.

Geneva, Switzerland
September, 2007

Compressor lattice design for SPL beam
31/Aug/2007
Masamitsu Aiba

1. Introduction

A compressor ring providing very short proton bunches of a few ns has been designed as a component of a proton driver in the neutrino factory. Proton beams accelerated with the SPL (Superconducting Proton Linac [1]) are stored in an accumulator ring [2] before being transported to a compressor ring. The bunch compression is then performed with longitudinal phase rotation. For the neutrino factory, a special pulse structure of the primary proton beam is required. In the SPL based proton driver, the specification imposes that six (or five) bunches of a few ns length and about 12μs bunch spacing are formed in one cycle.

2. Specifications of the compressor ring

In order to realize the pulse structure within the proposed accumulation and compression scenario [3], the following specifications are imposed to the compressor ring:

1) the kinetic energy of 5 GeV(±5 MeV), provided by the SPL,
2) the circumference of 100π m,
3) the slippage factor of 0.164 (= the transition gamma of 2.3),
4) sufficient straight section for rf cavities, injection and extraction devices,
5) the dispersion function as small as possible all over the ring.

The circumference of the ring has been determined taking into account the performance of the phase rotation. It is assumed that the phase rotation takes 36 turns and that the six accumulated bunches are injected into the compressor ring bunch by bunch every 1/3 period of the phase rotation. In this scenario, the bunch spacing corresponds to 12 turns and the revolution period should be about 1 μs. Thus, the circumference is about 300 m.

In order to achieve the rapid phase rotation for 36 turns, the slippage factor should be large enough. When we assume 4 MV total rf voltage, the slippage factor should be 0.164. It corresponds to the transition gamma of 2.3 for the kinetic energy of 5 GeV. This number results in a rotation by more than 90 degrees but is found with the 1-dimensional tracking simulation [3] to minimize the bunch length taking into account the nonlinear force of sine wave. Most of the straight section will be occupied by rf cavities to obtain a total rf voltage of 4 MV. RF cavities under vacuum with large capacitive loading could be used. A straight section of 40 m has been allocated to the RF systems (real estate gradient: 100 kV/m).

The dispersion function should be as small as possible to keep a realistic size of the ring aperture. The aperture of ring is mainly determined by the dispersion term $D\,dP/P$ since the momentum spread is increased by ~±1.6% after phase rotation in a 4 MV rf bucket.

3. Dispersion function and slippage factor

Small dispersion function and large slippage factor are conflicting because of their relationship through the momentum compaction,

$$\eta = \frac{1}{\gamma_{tr}^{\ 2}} - \frac{1}{\gamma^2} \quad , \tag{1}$$

$$\frac{1}{\gamma_{tr}^{\ 2}} = \alpha_p = \frac{1}{C}\int_0^C \frac{D(s)}{\rho(s)} ds \, , \tag{2}$$

where η is the slippage factor, γ_{tr} is the transition gamma, γ is the relativistic factor, α_p is the momentum compaction factor, C is the circumference, D is the horizontal dispersion function and ρ is the curvature radius.

Since the curvature radius is infinite outside of bending magnet we get,

$$\alpha_p = \frac{L}{C}\frac{\overline{D}}{\rho} = \frac{\overline{D}}{\overline{R}}, \tag{3}$$

where L is the total length of bending magnets, $\overline{D}$ is the average value of dispersion function within bending magnets, and $\overline{R}$ is the equivalent radius of ring. To reach the slippage factor of 0.164 (α_p=0.189), the average dispersion over the bending magnets should be,

$$\overline{D} = \alpha_p \overline{R} = 0.189 \times 50 = 9.45m \tag{4}$$

The dispersion function of 9.45 m seems rather large because it leads to orbit excursion of

$$\pm \Delta x = D\frac{dP}{P} = \pm 9.45m \times 0.016 = \pm 0.15m \tag{5}$$

By introducing negative bending magnets in the lattice where the dispersion function is negative, the dispersion function could be smaller without reducing the target slippage factor. For instance, the total length of bending magnet L in Eq. 3 is increased and the average dispersion could be reduced. Obviously, the dispersion function should oscillate from negative to positive value, and the lattice will be complicated. We will investigate two possibilities, a lattice without negative bending magnets and a lattice with negative bending magnets.

4. Lattice without negative bending magnets

Since some parameters such as the circumference and the slippage factor are fixed, other parameters are restricted to fit them. To survey basic parameters, the transition gamma and the dispersion function in a FODO cell are calculated for various numbers of cells and phase advances as shown in Fig. 1. The number of cells would be around eight, and then the dispersion is about 12 m which is roughly consistent with Eq. 4.

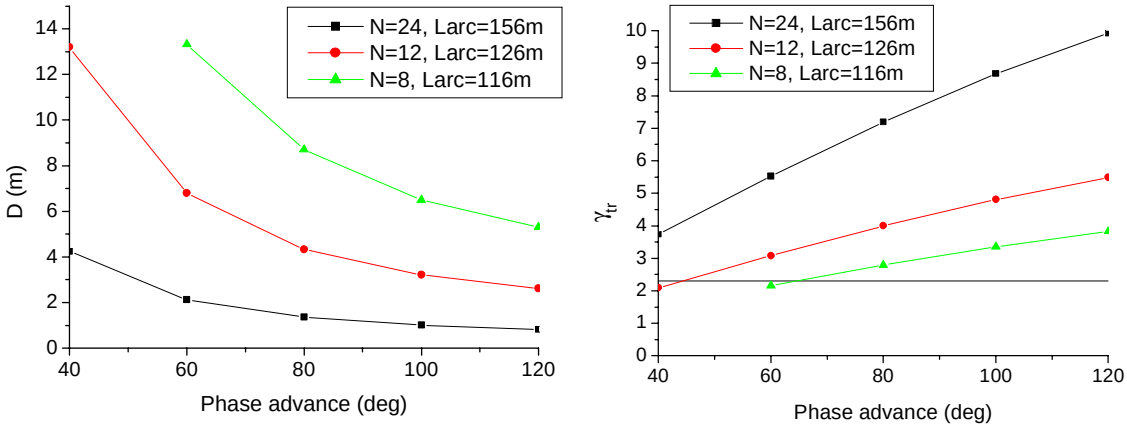

Figure 1. Dispersion function and transition gamma in FODO cell for various phase advances and numbers of cells

Equation 2 implies that the ideal location of bending magnets is the place of maximum dispersion function. If the modulation of the dispersion function is weak, this condition is achieved to some extent. Triplet FDF is better to flatten the dispersion than FODO. A lattice function with FDF triplet is calculated and shown in Fig. 2. When the slippage factor is 0.164 the maximum dispersion function of the lattice is 10.24 m while the ideal one is 9.45 m. The allocation of dipoles is very efficient in the lattice.

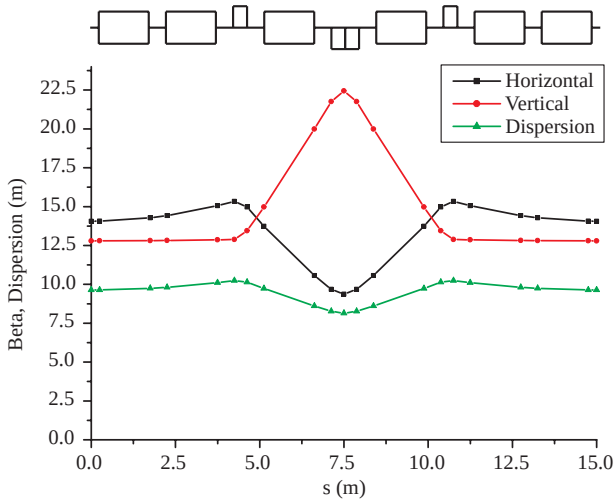

Figure 2. Lattice function for FDF triplet (N=8)

In straight sections, the dispersion function is ideally expected to be zero for the insertions. Generally, the dispersion suppressor is employed between the arc cell and the straight section. Figure 3 shows an example of dispersion suppressor for triplet FDF with missing magnet cell.

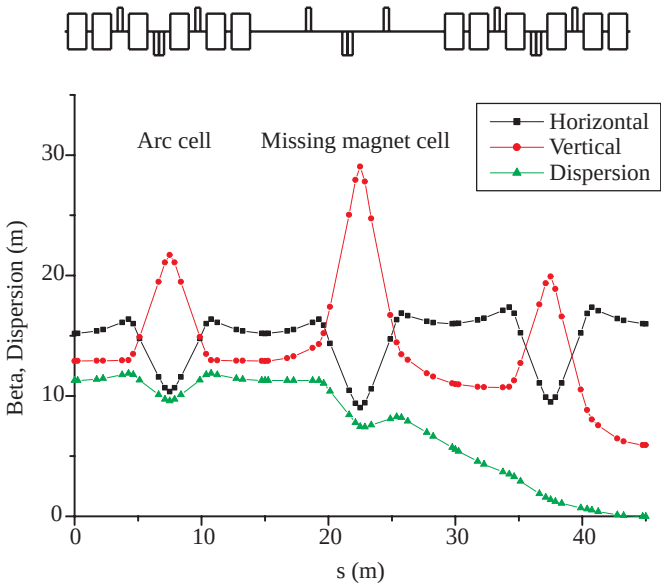

Figure 3. Dispersion suppressor with missing magnet cell.
The horizontal phase advance per cell is 60 degrees.

The dispersion suppressor is, however, not a possible solution as it reduces the slippage factor significantly when the number of cells is small. When the number of arc cells is eight, in a racetrack ring, half of the bending magnets should be after the missing magnet cell where the dispersion function is decreasing to zero. If the number of cells is increased, the ratio of number of bending magnets in the dispersion suppressor to the ones in the arc cells decreases. However, the phase advance should be reduced not to change the slippage factor, and negative bending magnets have to be added in the dispersion suppressor, which results in the reduction of slippage factor. In the end, the dispersion function in the arc cells should be increased significantly when the dispersion suppressor is employed. Due to consequences on the magnet apertures, this solution is not attractive.

While the dispersion suppressor is not retained, it could be used to contain the oscillation of the dispersion function around acceptable level for insertions. Figure 4 shows an example of straight section based on this concept.

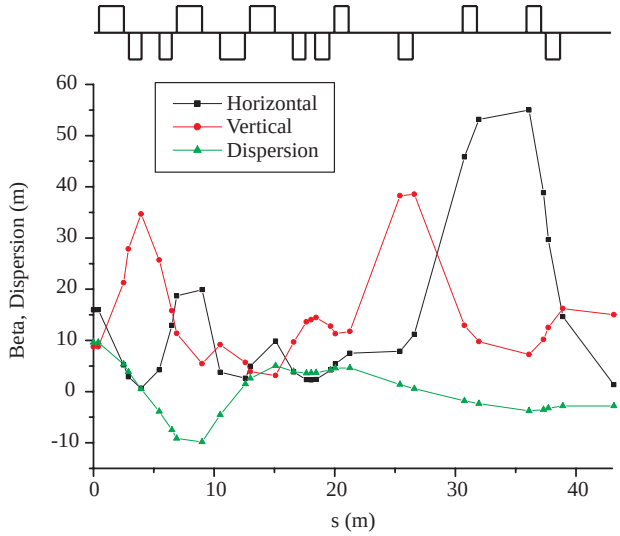

Figure 4. Half straight section with oscillating dispersion function

The dispersion function, more than 20 m away from the end of arc cell, is reduced to less than 4.5 m. It must be noted that the lattice in Figure 4 has not been well elaborated. Since the length of straight section to the arc cell is relatively long, there are a lot of possible configurations for quadrupole magnets.

Further studies are necessary to confirm the feasibility from the viewpoints of magnet apertures and beam dynamics. The maximum dispersion function of 10.4m results in large magnet apertures, which more or less enhance the beam dynamics issues related to the fringe field and unexpected allowed multi-poles. At this moment, we regard this lattice as the second option because it seems reasonable to have smaller dispersion function with negative bending magnets.

5. Lattice with negative bending magnets

By introducing negative bending magnets, the maximum dispersion function is reduced significantly. If we assume that the total length of bending magnets is doubled, that is, 150% positive bending and –50% negative bending, the dispersion function could ideally be reduced to ±4.73 m.

Since the dispersion function should be negative at the negative bending to contribute to the integral of Eq. 2, one arc cell will be composed of three functional parts, a cell with positive bending magnets, a cell with negative bending magnets and a cell that flips the sign of dispersion function. We call the third one “matching cell” hereafter in this note. The phase advance of the matching cell is preferably close to 180 degrees so that the dispersion function oscillates symmetrically about zero. Therefore relatively long (strong) quadrupole magnets are necessary in the matching cell.

Due to not only the increased total length of bending magnets but also the length of the matching cell, the total length for the magnets is almost doubled compared to the one in the lattice without negative bending. It is estimated to be about 260 m (including the spaces between magnets) when we assume normal conducting bending magnets of 1.8 T. The straight section will be about 50 m, which is too short for the insertions. Therefore we assume to use superconducting bending magnets. Figure 5 shows one arc cell with the superconducting bending magnets of 5.1 T.

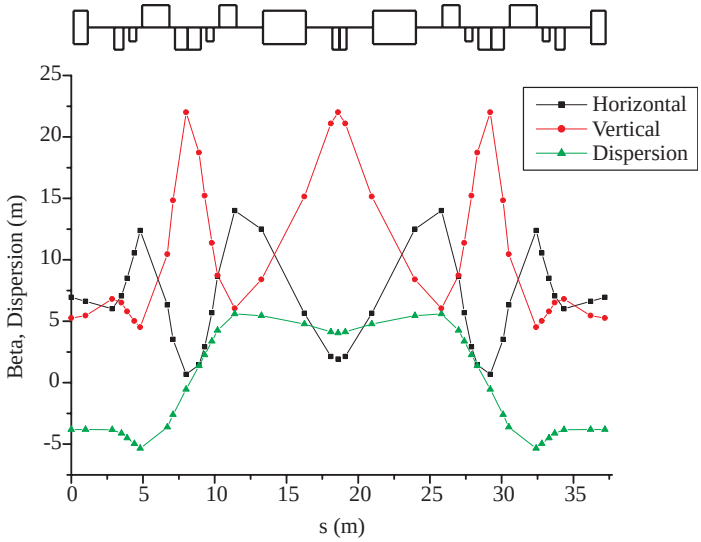

Figure 5. Arc cell with positive and negative bending magnets
Spaces of 1.85m are retained at the both ends of superconducting magnets. They are necessary for the coil-ends, connections, etc.

In Fig. 5, the maximum dispersion is 5.53 m, which is effectively reduced by introducing the negative bending. The phase advance of the matching cell is about 140 degrees but the dispersion function oscillates almost symmetrically about zero by shaking down the phase advances of other two cells. We started with the cell number of eight and finally arrived at six after some optimizations.

Since the momentum spread after phase rotation is significant, the chromaticity correction is necessary. The chromatic tune shift will respectively be ±0.234 and ±0.132 in horizontal and vertical plane, if no correction is applied. The chromaticity correction sextupoles are therefore installed in the lattice, using two focusing and two defocusing sextupoles in each arc cells. The betatron tunes with chromaticity correction are almost constant over the momentum spread after phase rotation.

Introduction of a dispersion suppressor is not possible due to the same reason as for the lattice without negative bending magnets. The lattice of the straight section is designed with oscillating dispersion function as shown in Fig. 6.

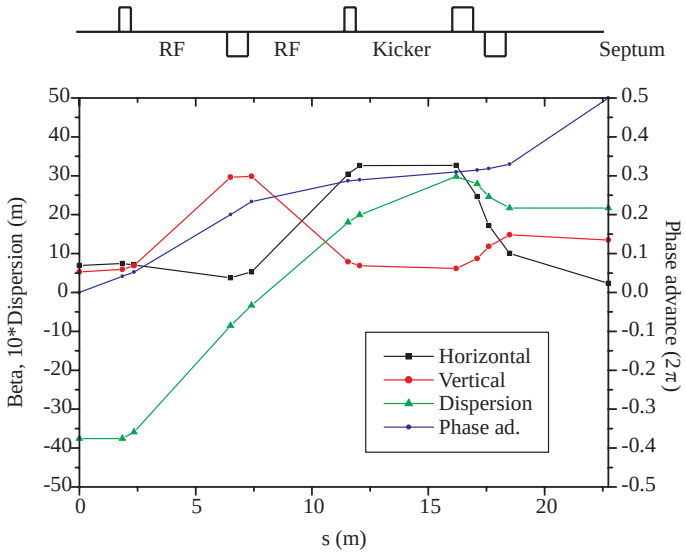

Figure 6. Half straight section

The straight section of 41.5 m in total (10*4.15 m) is secured for the rf cavities. The injection and extraction kickers are to be accommodated in 4.15 m straight section, and the septa in about 8 m straight section.

For the completeness, Fig. 7 shows the lattice of whole ring and the specification of the magnets in the arc cells are estimated in Table 1.

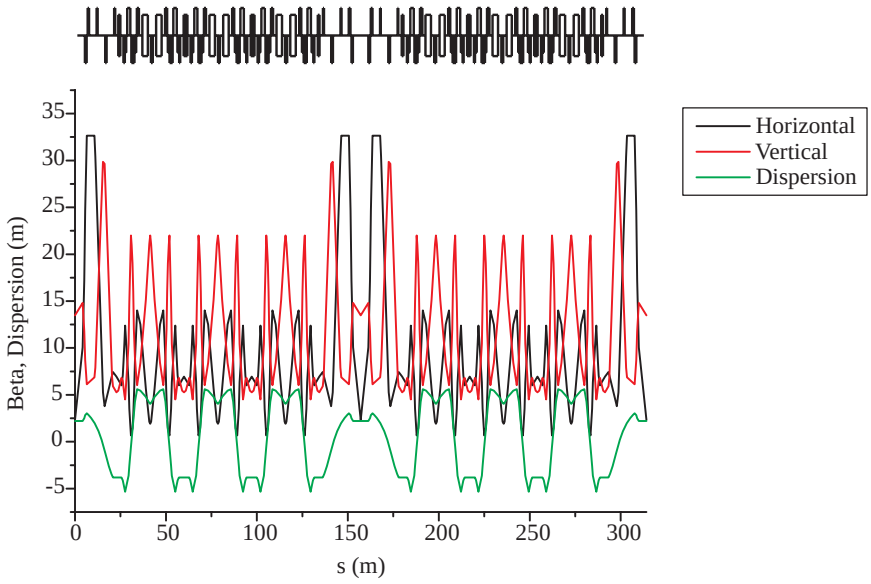

Figure 7. Compressor lattice with negative bending magnets

Table 1. Estimation of the magnet specifications

The strongest and longest magnets are listed. The superconducting bending magnet would be feasible with small extension of present technology, as indicated in reference [4].

Emittance (Gaussian r.m.s., H/V)		1.25/2.5 (πmm-mrad)
dP/P		±1.6%
Quadrupole		Half beam size
Beta_x (120%)	16.8 m	27.5 mm
Dx (110%)	6.083 m	97.3 mm
COD		5 mm
Mechanical tolerance		3 mm
Chamber		5 mm
Bore radius	138 mm	
Field gradient	~7.3 T/m	
Field at pole tip	~1T	
Length	1.9 m	
Bending		Half beam size
Beta_x (120%)	16.8 m	27.5 mm
Dx (110%)	6.08 m	97.3 mm
COD		5 mm
Mechanical tolerance		3 mm
Chamber		10 mm
Good field		80%
Horizontal aperture (full)	357 mm	
Beta_y (120%)	26.4 m	48.7 mm
COD		5 mm
Mechanical tolerance		3 mm
Chamber		10 mm
Vertical gap (full)	133 mm	
Field strength	~5.1 T	
Length	3 m	

6. Tracking simulation

Since the peak current after phase rotation will be significantly large, we need to carefully investigate the space charge effects. First the space charge tune shift (Laslett tune shift in free space) is estimated analytically for a Gaussian distribution with the line density corresponding to the injection beam.

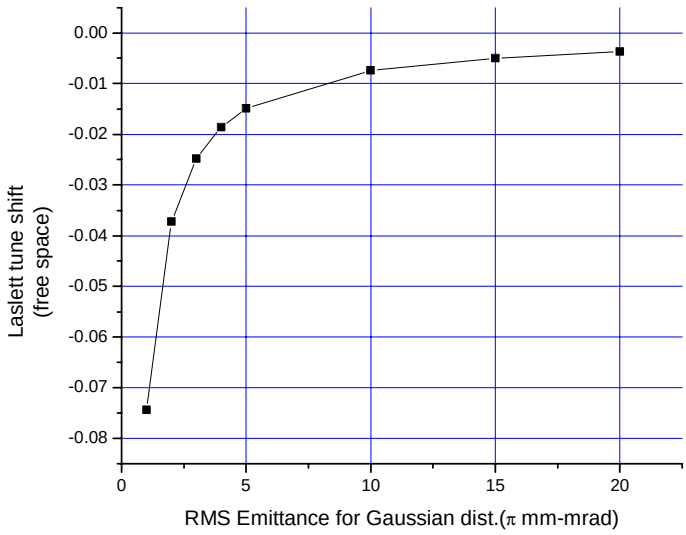

Figure 8. Laslett tune shift vs. r.m.s. emittance for Gaussian distribution

$$\Delta\nu = -\frac{n_p r_p}{4\pi\varepsilon\beta^2\gamma^3}$$

The same beam size both in horizontal and vertical plane is assumed.
The peak line density is 4.69E11 /m.

If we assume that the tune shift is simply proportional to the line density, the tune shift after the phase rotation in a 4 MV rf bucket is approximately 17 times larger than that of the injection beam since the energy spread is increased from ±5 MeV to ±85 MeV. The r.m.s. beam emittance is then preferred to be more than 5π mm-mrad so that the tune shift does not exceed 0.25.

However this estimation easily fails in the compressor ring because of the rather large dispersion function and momentum spread after phase rotation. Since the horizontal beam size is mainly determined by the dispersion term $D\,dP/P$, the space charge tune shift is not correctly estimated as far as the beam size is expressed as a function of the amplitude of the betatron oscillation only.

To confirm this fact, tracking simulation with ORBIT code, in which transverse and longitudinal space charge forces are calculated based on 2.5-dimensional PIC (Particle-In-Cell) method, is performed. The lattice shown in Fig. 7 is inputted to ORBIT. The elliptical distribution instead of Gaussian distribution is used to confine particles to finite amplitude. The r.m.s. beam emittances are respectively 1π mm-mrad and 2π mm-mrad in horizontal and vertical plane. The longitudinal distribution is flat in phase and parabolic in energy to model the beam characterized by the SPL. Figure 9 shows the results of simulation.

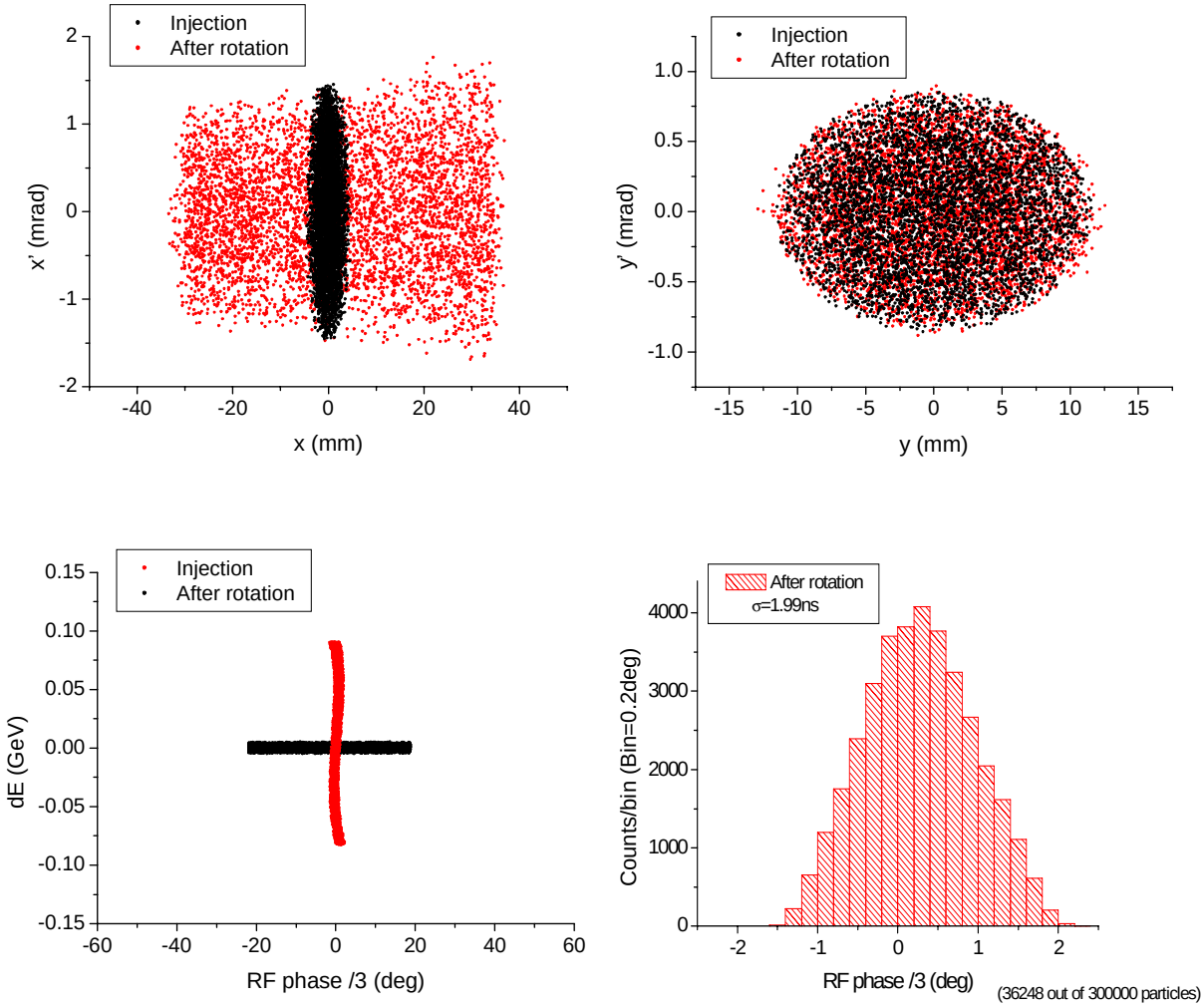

Figure 9. Simulation results: phase spaces and bunch profile
The rf voltage and the initial longitudinal beam position are adjusted as 3.9 MV and ±20.4deg.-1.5deg. (120 ns) to minimize the bunch length after phase rotation.

The bunch length is successfully shortened to less than 2 ns with phase rotation. The vertical emittance seems to increase a bit during phase rotation but this would be just an appearance of the beta function variation over the momentum spread. In the horizontal plane, the beam size is effectively expanded by the dispersion term.

The space charge tune shift is calculated with the interpolated FFT over 32 turns tracking. Since the phase rotation changes line density rapidly, the rf voltage is turned off for the FFT tune calculation. Even then, the line density of the bunched beam is not constant due to the drift without longitudinal focusing force. Therefore the coasting

beams, which have line densities corresponding to the ones before and after phase rotation, are employed. The line density after phase rotation is set to the peak density obtained (1.1E13 /m) from Fig. 9. The longitudinal space charge force is excluded in coasting beam but this simulation is good enough to explore the reduction of space charge tune shift due to the dispersion term. Figure 10 shows the tune spread and Table 2 summarizes the tune shift together with analytical values.

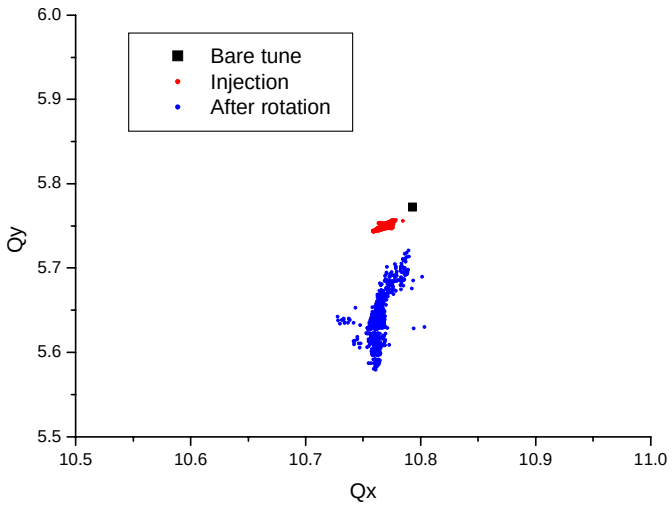

Figure 10. Tune spread before and after phase rotation

Table 2. Space charge tune shift

Different beam sizes for horizontal and vertical is assumed. In analytic value, beam size is simply calculated as a function of the betatron amplitude only.

	Simulation (H/V)	Analytic (H/V)
Injection	~0.033/~0.029	0.0397/0.0384
After rotation	~0.063/~0.19	0.929/0.898

$$\Delta\nu = -\frac{n_p r_p}{2.5\pi\beta^2\gamma^3}\frac{<\beta_i>}{\sigma_i(\sigma_i+\sigma_j)}$$

$$(i,j) = (x,y) or (y,x)$$

The tune shift is much smaller than the analytic ones as shown in Table 2. It is noteworthy that the effect of dispersion term is larger in the horizontal plane than in the vertical. When the horizontal beam size is expanded, the vertical beam size does not change but the particle density in the real space decreases inversely proportional to the horizontal beam size. Therefore the vertical space charge force will also decrease proportionally to the horizontal beam size. On the other hand, the horizontal space charge force is inversely proportional to the square of the horizontal beam size. This might partly explain the large difference between the horizontal and vertical tune shift.

Through the effect of the dispersion term, it is possible to inject the relatively small beam emittance in the compressor. We assume Gaussian distribution again to be

pessimistic for the aperture estimation and choose the r.m.s. beam emittance of respectively 1.25π mm-mrad and 2.5π mm-mrad in horizontal and vertical plane, as in Table 1, so that the tune shifts are the same to the ones of elliptic distribution in the simulation.

7. Summary

We have found a possible lattice for the compressor ring. All of the specifications on the pulse structure, about 2 ns bunch width and about 12 μs bunch spacing, are met with the proposed lattice. The maximum dispersion function of 5.5 m is achieved by introducing negative bending magnets and assuming 5.1 T superconducting bending magnets. We also found that the space charge tune shift is much less proportional to the line density in the compressor ring because the horizontal beam size is expanded by the dispersion term. The corresponding r.m.s. beam emittance of respectively 1.25π mm-mrad and 2.5π mm-mrad in the horizontal and vertical planes are acceptable.

8. Acknowledgement

I would like to thank Dr. R. Garoby for introducing me to this work, continuous support and many helpful comments. I wish to thank Dr. M. Meddahi for valuable discussions, double-checks of MAD input and supports to finish this note. I also thank Dr. W. Herr for useful comments based on his wide knowledge of MAD program and lattice design. Dr. C. Carli has given me advice and help for the simulation of phase rotation. For the design of straight section, I want to thank Dr. B. Goddard for his help. I would like to acknowledge Dr. T. Nakamoto for valuable discussions concerning superconducting magnet. Last but not least, I am grateful to Drs. S. Cousineau and A. Shishlo for their kind supports on ORBIT simulation.

References

[1] F. Gerick (ed.) et. al., CERN-2006-006
[2] M. Aiba, CERN- AB/BI note and CERN-NUFACT-Note-151
[3] R. Garoby, Presentation at NuFact'06, https://edms.cern.ch/document/808094/1
[4] H. Okuno et. al., IEEE Transaction on Applied Superconductivity, Vol.12, No.1, pp192-195 (2002)